

Electromagnetic scattering by fully ordered and quasi-random rigid particulate samples

MICHAEL I. MISHCHENKO,^{1,*} JANNA M. DLUGACH,² AND DANIEL W. MACKOWSKI³

¹NASA Goddard Institute for Space Studies, 2880 Broadway, New York, New York 10025, USA

²Main Astronomical Observatory of the National Academy of Sciences of Ukraine, 27 Zabolotny Str., 03680 Kyiv, Ukraine

³Department of Mechanical Engineering, Auburn University, Alabama 36849, USA

*Corresponding author: michael.i.mishchenko@nasa.gov

Received 8 August 2016; revised 15 September 2016; accepted 15 September 2016; posted 16 September 2016 (Doc. ID 273330); published 10 October 2016

In this paper we have analyzed circumstances under which a rigid particulate sample can behave optically as a true discrete random medium consisting of particles randomly moving relative to each other during measurement. To this end, we applied the numerically exact superposition T -matrix method to model far-field scattering characteristics of fully ordered and quasi-randomly arranged rigid multiparticle groups in fixed and random orientations. We have shown that, in and of itself, averaging optical observables over movements of a rigid sample as a whole is insufficient unless it is combined with a quasi-random arrangement of the constituent particles in the sample. Otherwise, certain scattering effects typical of discrete random media (including some manifestations of coherent backscattering) may not be accurately replicated. © 2016 Optical Society of America

OCIS codes: (290.5850) Scattering, particles; (030.6140) Speckle; (030.5620) Radiative transfer; (260.5430) Polarization.

<http://dx.doi.org/10.1364/JOSAA.33.002144>

1. INTRODUCTION

According to [1], the “optical” definition of a type-1 discrete random medium (DRM) is that it is a morphologically complex object in the form of an imaginary volume V populated by a large number N of small particles in such a way that the spatial distribution of the particles throughout the volume is maximally random and uniform in the statistical sense [2–10]. In “true” DRMs such as low-density suspensions of particles in gases and liquids, statistical randomness and uniformity are naturally achieved over a sufficiently long period as a result of random temporal changes of particle positions. To model light scattering by such objects, one needs to assume ergodicity and average the solution of the macroscopic Maxwell equations (MMEs) over a representative set of realizations of a multiparticle group. This so-called ensemble averaging (EA) serves to randomize phase relationships between various multiparticle sequences and thereby yields typical speckle-free patterns of time-averaged optical observables [1,10].

Furthermore, it is frequently assumed that the optical concept of a DRM can be applied to rigid particulate media such as powder surfaces, sheets of paper, layers of paint, and biological tissues. This assumption is usually invoked whenever the measured scattering patterns exhibit no speckles. For example, it has been demonstrated experimentally that rotating or vibrating an entire rigid particulate sample during the measurement results in characteristic speckle-free angular patterns of the

scattered light [11–13]. In this case, it is the movement of the sample as a whole relative to the source of light and the detector that causes the randomization of the phase relations between different multiparticle sequences. However, these experimental results, despite their qualitative importance, have not established the quantitative equivalence of the EA (i.e., the averaging over random individual-particle coordinates) and the averaging over movements of a rigid sample as a whole, which will be referred to as rigid-sample averaging (RSA).

This issue was partially resolved in [1,10,14] by using numerically exact computer solutions of the MMEs and implementing a two-step modeling procedure. First, researchers used a random-number generator of particle coordinates to render a rigid particulate sample in the form of an N -particle group quasi-randomly and quasi-uniformly populating a spherical volume V . Second, all far-field scattering characteristics of the rigid sample were averaged over the uniform distribution of its orientations with respect to the laboratory reference frame. It was found that upon orientation averaging, different (but N - and V -equivalent) computer renditions of the rigid particulate sample yielded virtually indistinguishable far-field scattering patterns.

That result can be viewed as a testimony to the quantitative equivalence the EA and the RSA and is, in fact, not surprising. Indeed, combining orientation averaging with the initial quasi-randomness of particle positions in a rigid-sample rendition can

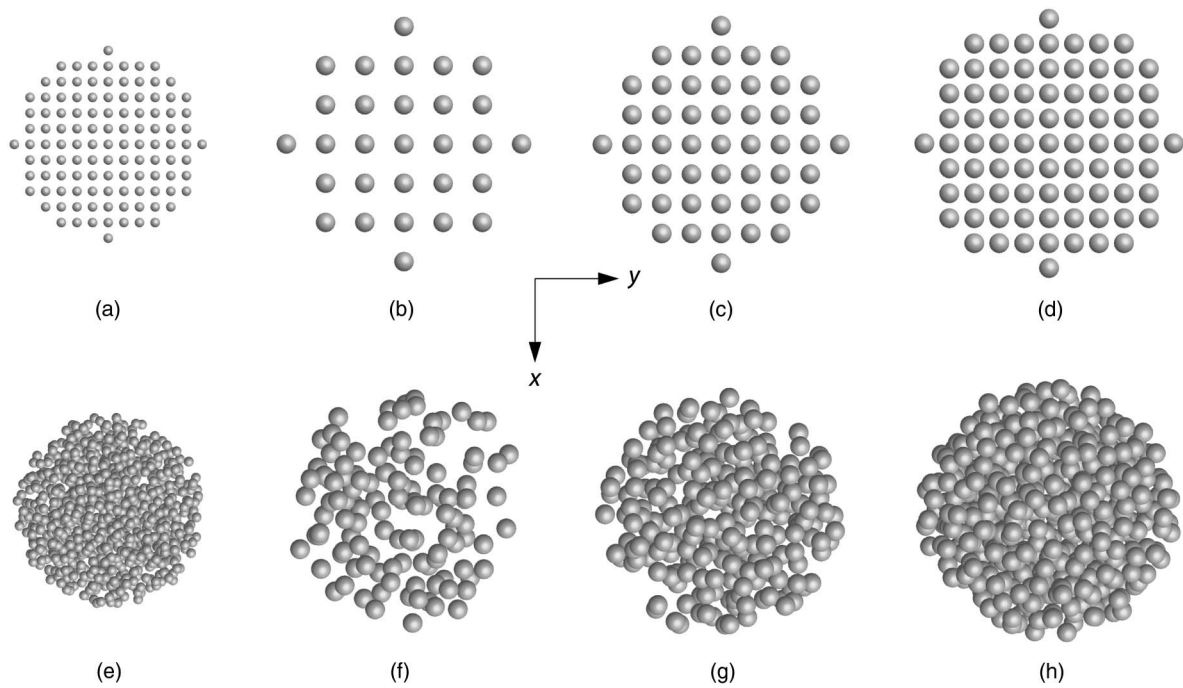


Fig. 1. Fully ordered (upper panels) and quasi-random (lower panels) rigid particulate samples as viewed by an observer looking in the negative direction of the z axis of the sample's reference frame.

qualitatively be thought of as yielding an infinite continuous set of random realizations of the N -particle group with respect to the laboratory coordinate system.

Importantly, however, the specific RSA simulations in [1,10,14] convolved the optical effect of averaging over sample orientations with that of the initial quasi-randomness and quasi-uniformity of particle positions resulting from the use of the random-number generator of particle coordinates. As a consequence, the relative importance of these two effects in causing EA-equivalent scattering patterns remained unknown.

A straightforward and simple way to deconvolve these two optical effects and establish definitively what makes a multiparticle group a DRM is to compare two limiting cases, i.e., fully ordered and quasi-random rigid multiparticle groups having the same N and V . As in [1,10,14], we performed this comparison by computing the relevant far-field optical observables using the numerically exact and computationally efficient superposition T -matrix solver of the MMEs [15,16].

2. MODELING METHODOLOGY

Figure 1 shows the eight rigid particulate samples analyzed in this paper. Each sample consisted of N identical particles populating a spherical volume V having a radius R . In all cases, the particles did not overlap and did not cross the spherical surface S serving as the boundary of the volume V . The particles in samples (a)–(d) were centered at the nodes of a regular cubic grid with S serving as the smallest circumscribing sphere of the corresponding multiparticle group. The particles in samples (e)–(h) were positioned quasi-randomly and quasi-uniformly using a random-number generator of particle coordinates. All particles have the same refractive index

$m = 1.32$ characteristic of liquid water and water ice at visible wavelengths. For the purposes of light-scattering computations, we characterized each sample by its size parameter $X = 2\pi R/\lambda$, where λ is the wavelength, and each particle by its size parameter $x = 2\pi r/\lambda$, where r is the particle radius. Table 1 summarizes the geometrical characteristics of the eight particulate samples, in which $\rho = Nr^3/R^3$ is the packing density. We chose the specific numbers in Table 1 to explore a representative range of model parameters while keeping the computational effort reasonable.

Consistent with [7,10], the time-averaged Stokes column vector of the scattered spherical wavefront (“sca”) in the far zone of a fixed particulate object is expressed in terms of the time-averaged Stokes column vector of the incident quasi-monochromatic plane wave (“inc”) via the 4×4 real-valued phase matrix \mathbf{Z} as

$$\mathbf{I}^{\text{sca}}(D\hat{\mathbf{n}}^{\text{sca}}) = \frac{1}{D^2} \mathbf{Z}(\hat{\mathbf{n}}^{\text{sca}}, \hat{\mathbf{n}}^{\text{inc}}, \lambda) \mathbf{I}^{\text{inc}}, \quad (1)$$

where $\hat{\mathbf{n}}^{\text{inc}} = \{\theta^{\text{inc}}, \varphi^{\text{inc}}\}$ is the unit vector in the incidence direction; $\hat{\mathbf{n}}^{\text{sca}} = \{\theta^{\text{sca}}, \varphi^{\text{sca}}\}$ is that in the scattering direction; D is the distance from the center of the object to the far-zone observation point; and $\{\theta, \varphi\}$ are the zenith and azimuth angles

Table 1. N - and V -Equivalent Pairs of Particulate Samples

Samples	X	x	N	ρ
(a) and (e)	41	2	925	0.107
(b) and (f)	52	4	123	0.056
(c) and (g)	52	4	257	0.117
(d) and (h)	54	4	515	0.209

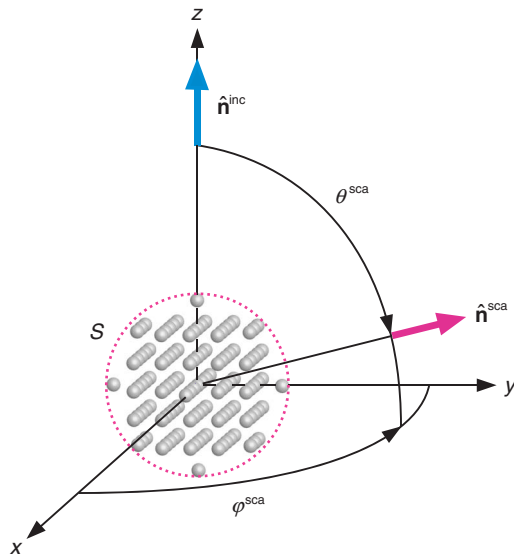


Fig. 2. Far-field scattering geometry. In this case, the fixed scattering object is the fully ordered sample (c).

of a propagation direction in the fixed (laboratory) spherical coordinate system centered at the object (Fig. 2). In what follows, we will assume that $\theta^{\text{inc}} = 0$, i.e., that the incident wavefront propagates in the positive direction of the z -axis.

Assuming also that the incidence and scattering directions belong to the xz plane (i.e., $\varphi^{\text{sca}} = \varphi^{\text{inc}} = 0$), the corresponding normalized scattering matrix is defined as

$$\tilde{\mathbf{F}}^{(1)}(\Theta) = C^{(1)} \mathbf{Z}(\theta^{\text{sca}} = \Theta, \varphi^{\text{sca}} = 0; \theta^{\text{inc}} = 0, \varphi^{\text{inc}} = 0), \quad (2)$$

where $C^{(1)}$ is a normalization constant and Θ is the scattering angle. In the case of a rigid sample in random orientation with respect to the laboratory reference frame, the normalized scattering matrix is defined according to

$$\tilde{\mathbf{F}}^{(2)}(\Theta) = C^{(2)} \langle \mathbf{Z}(\theta^{\text{sca}} = \Theta, \varphi^{\text{sca}} = 0; \theta^{\text{inc}} = 0, \varphi^{\text{inc}} = 0) \rangle, \quad (3)$$

where $\langle \dots \rangle$ denotes averaging over the uniform orientation distribution of the sample. The constants $C^{(1)}$ and $C^{(2)}$ are chosen such that the (1,1) element of each scattering matrix (conventionally referred to as the phase function) satisfies the standard normalization condition

$$\frac{1}{2} \int_0^\pi d\Theta \tilde{F}_{11}(\Theta) \sin \Theta = 1. \quad (4)$$

3. RIGID PARTICULATE SAMPLES IN A FIXED ORIENTATION

Let us first consider the situation wherein the orientation of a rigid particulate sample is fixed such that the axes of the sample's coordinate system coincide with those of the laboratory system (Fig. 2). Figure 3 visualizes a representative subset of the 16 elements of the scattering matrix $\tilde{\mathbf{F}}^{(1)}(\Theta)$ for the samples (a) and (e). Not surprisingly, the majority of the $\tilde{F}_{11}^{(1)}(\Theta)$ and $\tilde{F}_{ij}^{(1)}(\Theta)/\tilde{F}_{11}^{(1)}(\Theta)$ curves reveal pronounced speckle patterns in the form of irregular spike-like oscillations

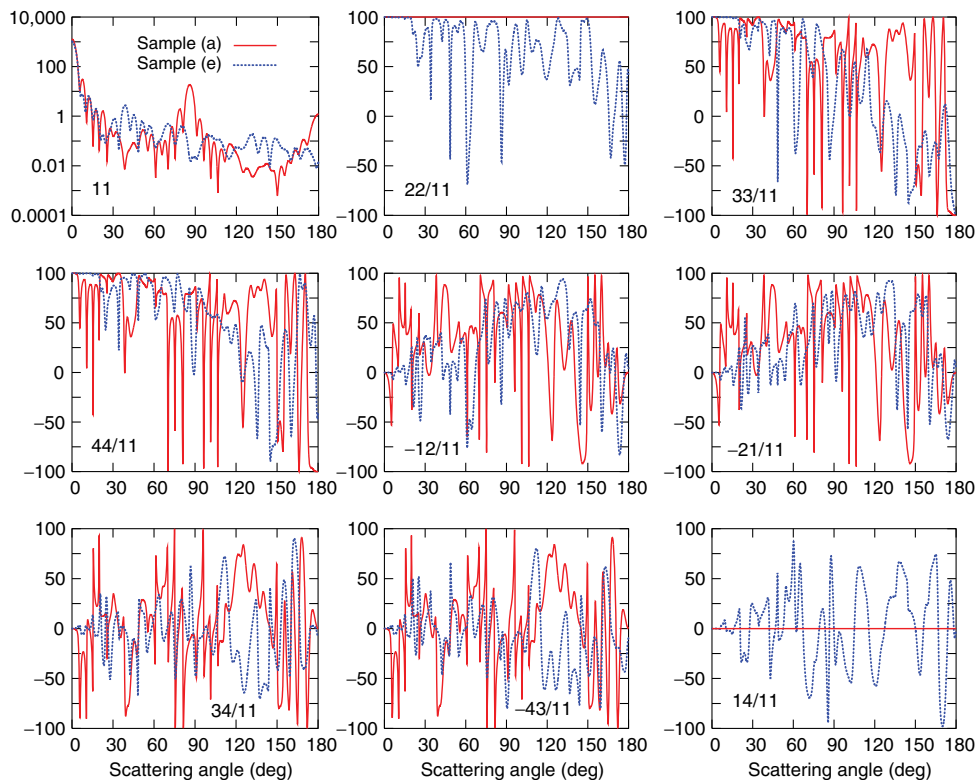


Fig. 3. Select elements of the normalized scattering matrix $\tilde{\mathbf{F}}^{(1)}(\Theta)$ for the samples (a) and (e). “11” denotes the phase function $\tilde{F}_{11}^{(1)}(\Theta)$, while “ $ij/11$ ” stands for $\tilde{F}_{ij}^{(1)}(\Theta)/\tilde{F}_{11}^{(1)}(\Theta)$ (%). Note that $\tilde{F}_{22}^{(1)}(\Theta)/\tilde{F}_{11}^{(1)}(\Theta) \equiv 100\%$ and $\tilde{F}_{14}^{(1)}(\Theta)/\tilde{F}_{11}^{(1)}(\Theta) \equiv 0$ for the sample (a).

[17,18]. However, there are two essential differences between the scattering properties of the two fixed samples.

First, the amplitude of the speckle oscillations is noticeably greater for the fully ordered sample (a). This is not surprising and can be explained in terms of the qualitative interpretation of speckles in the framework of the far-field Foldy formalism (see Section 18.2 of [10] or Section 8.1 of [1]). Indeed, in the case of a fully ordered particulate sample, there are many pairs of single- and/or multiparticle sequences having exactly the same phase difference between the respective pairs of light paths. This serves to magnify the corresponding cases of interference maxima or minima.

Especially instructive is the two-orders-of-magnitude difference in the corresponding $\tilde{F}_{11}(180^\circ)$ values. We observed similar $\tilde{F}_{11}(180^\circ)$ differences in the T -matrix results for the samples (b) and (f), (c) and (g), and (d) and (h) (not shown). The common origin of these differences is that the fully ordered samples in Fig. 1 can be viewed as consisting of parallel two-dimensional arrays (or layers) of particles confined to plains normal to the z axis (Fig. 2). As a consequence, the far-field wavelets singly scattered by particles from the same layer in the exact backscattering direction have exactly the same phase and always interfere constructively. This optical effect is analogous to the phenomenon of specular reflection from a perfectly flat interface and was first identified and analyzed in [19].

The cumulative waves backscattered by different layers interfere according to the respective phase differences, the overall backscattered intensity being dominated by a set of layers phase-separated from each other by values close to multiples of 2π . It is likely that the strong maximum exhibited by the sample (a) phase function at $\Theta \approx 90^\circ$ has a similar “specular-reflection” origin, i.e., is caused by layers of particles forming a 45° angle with the z axis.

There is another fundamental difference. On one hand, all 16 elements of the matrix $\tilde{\mathbf{F}}^{(1)}(\Theta)$ for the quasi-random sample (e) are nonzero and reveal no specific symmetries. On the other hand, the T -matrix results for the fully ordered sample (a) reveal (with an extremely high numerical accuracy) the following symmetric block-diagonal structure:

$$\tilde{\mathbf{F}}^{(1)}(\Theta) = \begin{bmatrix} \tilde{F}_{11}^{(1)}(\Theta) & \tilde{F}_{12}^{(1)}(\Theta) & 0 & 0 \\ \tilde{F}_{12}^{(1)}(\Theta) & \tilde{F}_{11}^{(1)}(\Theta) & 0 & 0 \\ 0 & 0 & \tilde{F}_{33}^{(1)}(\Theta) & \tilde{F}_{34}^{(1)}(\Theta) \\ 0 & 0 & -\tilde{F}_{34}^{(1)}(\Theta) & \tilde{F}_{33}^{(1)}(\Theta) \end{bmatrix} \quad (5)$$

with

$$\tilde{F}_{12}^{(1)}(0) = \tilde{F}_{34}^{(1)}(0) = \tilde{F}_{12}^{(1)}(\pi) = \tilde{F}_{34}^{(1)}(\pi) = 0, \quad (6)$$

$$\tilde{F}_{33}^{(1)}(0) = \tilde{F}_{11}^{(1)}(0), \quad \tilde{F}_{33}^{(1)}(\pi) = -\tilde{F}_{11}^{(1)}(\pi). \quad (7)$$

It is rather straightforward to show that this remarkable structure of the $\tilde{\mathbf{F}}^{(1)}(\Theta)$ matrix for the sample (a) is not a numerical artifact but rather follows rigorously from the MMEs. Indeed, mirroring this fully ordered sample with respect to the xz plane of the laboratory reference frame (i.e., the scattering plane) or rotating it through a 90° angle around the z axis results in exactly the same multiparticle configuration. As a consequence, the amplitude scattering matrix evaluated with

respect to the xz plane has the following symmetries (see Sections 5.2 and 5.3 of [20]):

$$\mathbf{S}(\Theta) = \begin{bmatrix} S_{11}(\Theta) & 0 \\ 0 & S_{22}(\Theta) \end{bmatrix}, \quad (8)$$

$$\mathbf{S}(0) = \begin{bmatrix} S_{11}(0) & 0 \\ 0 & S_{11}(0) \end{bmatrix}, \quad (9)$$

$$\mathbf{S}(\pi) = \begin{bmatrix} S_{11}(\pi) & 0 \\ 0 & -S_{11}(\pi) \end{bmatrix}. \quad (10)$$

It is then straightforward to verify that Eqs. (8)–(10) imply Eqs. (5)–(7).

4. RIGID PARTICULATE SAMPLES IN RANDOM ORIENTATION

Let us now consider the T -matrix results for the same rigid particulate samples but in random orientation. Now the mirror-symmetric morphology of the fully ordered samples implies the following structure of the normalized scattering matrix [7,10,20]:

$$\tilde{\mathbf{F}}^{(2)}(\Theta) = \begin{bmatrix} \tilde{F}_{11}^{(2)}(\Theta) & \tilde{F}_{12}^{(2)}(\Theta) & 0 & 0 \\ \tilde{F}_{12}^{(2)}(\Theta) & \tilde{F}_{22}^{(2)}(\Theta) & 0 & 0 \\ 0 & 0 & \tilde{F}_{33}^{(2)}(\Theta) & \tilde{F}_{34}^{(2)}(\Theta) \\ 0 & 0 & -\tilde{F}_{34}^{(2)}(\Theta) & \tilde{F}_{44}^{(2)}(\Theta) \end{bmatrix} \quad (11)$$

with

$$\tilde{F}_{12}^{(2)}(0) = \tilde{F}_{34}^{(2)}(0) = \tilde{F}_{12}^{(2)}(\pi) = \tilde{F}_{34}^{(2)}(\pi) = 0, \quad (12)$$

$$\tilde{F}_{33}^{(2)}(0) = \tilde{F}_{22}^{(2)}(0), \quad \tilde{F}_{33}^{(2)}(\pi) = -\tilde{F}_{22}^{(2)}(\pi), \quad (13)$$

$$\tilde{F}_{44}^{(2)}(\pi) = \tilde{F}_{11}^{(2)}(\pi) - 2\tilde{F}_{22}^{(2)}(\pi). \quad (14)$$

The T -matrix results for the sample (a) (Fig. 4) as well as for the samples (b)–(d) (not shown) perfectly reproduce this structure.

Furthermore, the structure described by Eqs. (11)–(14) is reproduced by the T -matrix results for the random samples (e)–(h) in the numerical sense. This means, in particular, that all off-block diagonal elements of the scattering matrix $\tilde{\mathbf{F}}^{(2)}(\Theta)$ are negligibly small (in the absolute-value sense) compared to the block-diagonal elements at the same scattering angle.

Despite this qualitative “structural” similarity, Fig. 4 reveals substantial quantitative differences between the scattering matrices computed for the samples (a) and (e). For example, the sample (a) phase function exhibits quasi-periodic order-of-magnitude oscillations at scattering angles exceeding $\sim 30^\circ$, while the sample (e) phase function is quite smooth. In general, Figs. 4 and 5 demonstrate that all scattering-matrix curves for the quasi-random particulate samples are much smoother and featureless than those for the N - and V -equivalent fully ordered samples. There is little doubt that the residual ripple in the solid

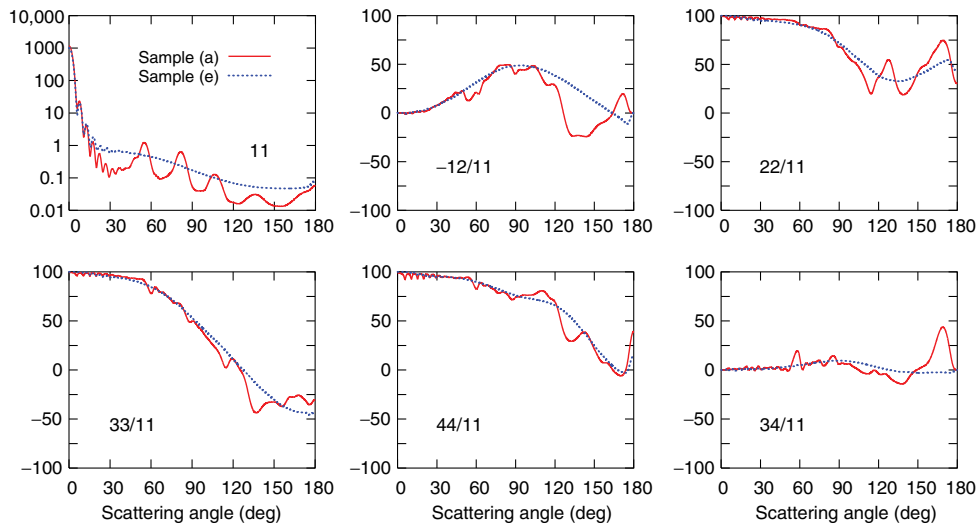


Fig. 4. As in Fig. 3, but for the normalized scattering matrix $\tilde{\mathbf{F}}^{(2)}(\Theta)$.

curves can be explained as the inability of orientation averaging to completely smooth out the more pronounced speckle patterns exhibited by fully ordered particulate samples in a fixed orientation.

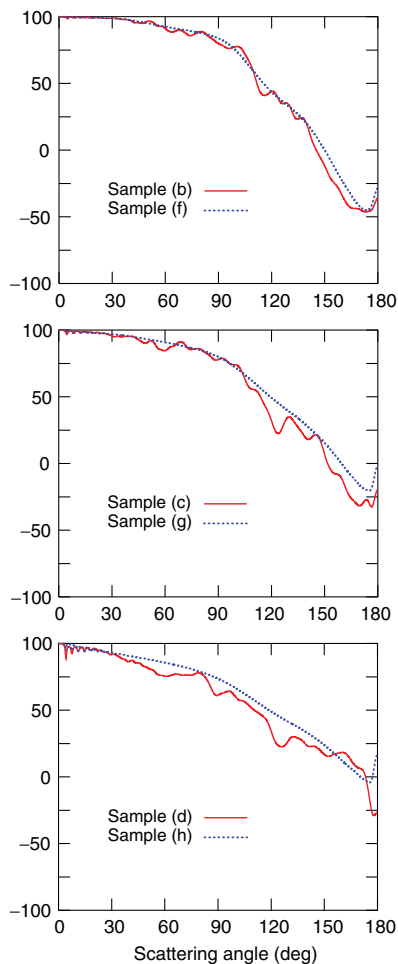


Fig. 5. Ratio $\tilde{F}_{44}^{(2)}(\Theta)/\tilde{F}_{11}^{(2)}(\Theta)$ for rigid particulate samples in random orientation.

The ratios $-\tilde{F}_{12}^{(2)}(\Theta)/\tilde{F}_{11}^{(2)}(\Theta)$ and $\tilde{F}_{34}^{(2)}(\Theta)/\tilde{F}_{11}^{(2)}(\Theta)$ for the samples (a) and (e) can differ at side- and near-backscattering angles to the extent of having opposite signs. In particular, the backscattering minimum in the $-\tilde{F}_{12}^{(2)}(\Theta)/\tilde{F}_{11}^{(2)}(\Theta)$ curve for the sample (e) is a specific manifestation of the phenomenon of coherent backscattering called the polarization opposition effect (POE) [21,22]. Instead of exhibiting the POE, the polarization curve for the sample (a) shows a near-backscattering positive-polarization maximum. This difference has a profound practical significance since the POE has actually been observed for certain natural and artificial particulate surfaces [23–27].

Finally, both $\tilde{F}_{44}^{(2)}(\Theta)/\tilde{F}_{11}^{(2)}(\Theta)$ curves in Fig. 4 exhibit backscattering peaks often attributed to coherent backscattering [1,10,14]. However, the $\tilde{F}_{44}^{(2)}(\Theta)/\tilde{F}_{11}^{(2)}(\Theta)$ curve for the sample (d) in Fig. 5 shows that full ordering of particles can cause a backscattering minimum instead of the more typical backscattering surge. This factor can affect the interpretation of active remote-sensing observations of particulate surfaces (e.g., [28–31] and references therein).

5. CONCLUDING REMARKS

Our main objective was to establish when a rigid particulate sample can behave optically as a true DRM in the form of a large group of particles randomly moving relative to each other during measurement. To answer this question, we used the superposition T -matrix method to compute the far-field scattering characteristics of rigid multiparticle samples consisting of fully ordered and quasi-randomly arranged particles. To model the movement of a rigid sample as a whole during measurement, we averaged the far-field optical observables over the uniform orientation distribution of the sample relative to the laboratory reference frame.

Not surprisingly, our T -matrix results for N - and V -equivalent pairs of fully ordered and quasi-random rigid samples in a fixed orientation revealed stark quantitative and qualitative differences. Averaging over orientations of fully ordered and quasi-randomly arranged rigid samples yields far-field scattering matrices having essentially the same mathematical structure and symmetry properties. Yet the corresponding angular patterns

of non-zero matrix elements reveal profound quantitative differences. In particular, we have found that fully ordered samples may not exhibit certain typical manifestations of coherent backscattering.

Therefore, we have concluded that averaging optical observables over movements of a rigid particulate sample as a whole during measurement is insufficient to replicate the scattering properties of a true DRM and must be combined with a quasi-random arrangement of the constituent particles in the sample.

Funding. National Aeronautics and Space Administration (NASA); National Academy of Sciences of Ukraine (NASU).

Acknowledgment. Funding was provided by the NASA Remote Sensing Theory Program and the National Academy of Sciences of Ukraine via the Main Astronomical Observatory GRAPE/GPU/GRID Computing Cluster Project. We appreciate numerous insightful discussions with Viktor Tishkovets, Larry Travis, and Gordon Videen and thank Alexandra Ivanova and Nadezhda Zakharova for help with Fig. 1. We also thank two anonymous reviewers for their constructive comments.

REFERENCES

- M. I. Mishchenko, J. M. Dlugach, M. A. Yurkin, L. Bi, B. Cairns, L. Liu, R. L. Panetta, L. D. Travis, P. Yang, and N. T. Zakharova, "First-principles modeling of electromagnetic scattering by discrete and discretely heterogeneous random media," *Phys. Rep.* **632**, 1–75 (2016).
- A. Ishimaru, *Wave Propagation and Scattering in Random Media* (Academic, 1978).
- L. Tsang, J. A. Kong, and R. T. Shin, *Theory of Microwave Remote Sensing* (Wiley, 1985).
- A. P. Ivanov, V. A. Loiko, and V. P. Dik, *Propagation of Light in Densely Packed Disperse Media* (Nauka i Tekhnika, 1988) (in Russian).
- L. Tsang, J. A. Kong, and K.-H. Ding, *Scattering of Electromagnetic Waves: Theories and Applications* (Wiley, 2000).
- V. A. Babenko, L. G. Astafyeva, and V. N. Kuzmin, *Electromagnetic Scattering in Disperse Media: Inhomogeneous and Anisotropic Particles* (Springer, 2003).
- M. I. Mishchenko, L. D. Travis, and A. A. Lacis, *Multiple Scattering of Light by Particles: Radiative Transfer and Coherent Backscattering* (Cambridge University, 2006), <http://www.giss.nasa.gov/staff/mmishchenko/books.html>.
- V. P. Tishkovets, E. V. Petrova, and M. I. Mishchenko, "Scattering of electromagnetic waves by ensembles of particles and discrete random media," *J. Quant. Spectrosc. Radiat. Transfer* **112**, 2095–2127 (2011).
- V. P. Tishkovets and E. V. Petrova, "Light scattering by densely packed systems of particles: near-field effects," in *Light Scattering Reviews* **7** (2013), pp. 3–36.
- M. I. Mishchenko, *Electromagnetic Scattering by Particles and Particle Groups: An Introduction* (Cambridge University, 2014).
- S. Etemad, R. Thompson, and M. J. Andrejco, "Weak localization of photons: universal fluctuations and ensemble averaging," *Phys. Rev. Lett.* **57**, 575–578 (1986).
- M. Kaveh, M. Rosenbluh, I. Edrei, and I. Freund, "Weak localization and light scattering from disordered solids," *Phys. Rev. Lett.* **57**, 2049–2052 (1986).
- R. Lenke and G. Maret, "Multiple scattering of light: coherent backscattering and transmission," in *Scattering in Polymeric and Colloidal Systems*, W. Brown and K. Mortensen, eds. (Gordon and Breach, 2000), pp. 1–73.
- M. I. Mishchenko, L. Liu, D. W. Mackowski, B. Cairns, and G. Videen, "Multiple scattering by random particulate media: exact 3D results," *Opt. Express* **15**, 2822–2836 (2007).
- D. W. Mackowski and M. I. Mishchenko, "Calculation of the T matrix and the scattering matrix for ensembles of spheres," *J. Opt. Soc. Am. A* **13**, 2266–2278 (1996).
- D. W. Mackowski and M. I. Mishchenko, "A multiple sphere T-matrix Fortran code for use on parallel computer clusters," *J. Quant. Spectrosc. Radiat. Transfer* **112**, 2182–2192 (2011).
- J. W. Goodman, *Speckle Phenomena in Optics: Theory and Applications* (Roberts & Company, 2007).
- J. C. Dainty, *Laser Speckle and Related Phenomena* (Springer, 1975).
- A. Penttilä, "Quasi-specular reflection from particulate media," *J. Quant. Spectrosc. Radiat. Transfer* **131**, 130–137 (2013).
- H. C. van de Hulst, *Light Scattering by Small Particles* (Wiley, 1957).
- M. I. Mishchenko, J.-M. Luck, and T. M. Nieuwenhuizen, "Full angular profile of the coherent polarization opposition effect," *J. Opt. Soc. Am. A* **17**, 888–891 (2000).
- M. I. Mishchenko, J. M. Dlugach, L. Liu, V. K. Rosenbush, N. N. Kiselev, and Yu. G. Shkuratov, "Direct solutions of the Maxwell equations explain opposition phenomena observed for high-albedo solar system objects," *Astrophys. J.* **705**, L118–L122 (2009).
- B. Lyot, "Research on the polarization of light from planets and from some terrestrial substances," *NASA Tech. Transl. F-187* (NASA, 1964).
- V. K. Rosenbush, V. V. Avramchuk, A. E. Rosenbush, and M. I. Mishchenko, "Polarization properties of the Galilean satellites of Jupiter: observations and preliminary analysis," *Astrophys. J.* **487**, 402–414 (1997).
- Yu. Shkuratov, A. Ovcharenko, E. Zubko, O. Miloslavskaya, K. Muinonen, J. Piironen, R. Nelson, W. Smythe, V. Rosenbush, and P. Helfenstein, "The opposition effect and negative polarization of structural analogs for planetary regoliths," *Icarus* **159**, 396–416 (2002).
- V. K. Rosenbush and M. I. Mishchenko, "Opposition planetary phenomena in planetary astrophysics: observational results," in *Polarimetric Detection, Characterization, and Remote Sensing*, M. I. Mishchenko, Ya. S. Yatskiv, V. K. Rosenbush, and G. Videen, eds. (Springer, 2011), pp. 409–436.
- V. Rosenbush and N. Kiselev, "Icy moons of the outer planets," in *Polarimetry of Stars and Planetary Systems*, L. Kolokolova, J. Hough, and A.-C. Levasseur-Regourd, eds. (Cambridge University, 2015), pp. 340–359.
- S. J. Ostro, "Planetary radar astronomy," *Rev. Mod. Phys.* **65**, 1235–1279 (1993).
- M. I. Mishchenko and L. Liu, "Electromagnetic scattering by densely packed particulate ice at radar wavelengths: exact theoretical results and remote-sensing implications," *Appl. Opt.* **48**, 2421–2426 (2009).
- A. Virkki and K. Muinonen, "Radar scattering by planetary surfaces modeled with laboratory-characterized particles," *Icarus* **269**, 38–49 (2016).
- G. W. Patterson, A. M. Stickle, F. S. Turner, J. R. Jensen, D. B. J. Bussey, P. Spudis, R. C. Espiritu, R. C. Schulze, D. A. Yocky, D. E. Wahl, M. Zimmerman, J. T. S. Cahill, M. Nolan, L. Carter, C. D. Neish, R. K. Raney, B. J. Thomson, R. Kirk, T. W. Thompson, B. L. Tise, I. A. Erteza, and C. V. Jakowatz, "Bistatic radar observations of the Moon using Mini-RF on LRO and the Arecibo observatory," *Icarus*, doi: 10.1016/j.icarus.2016.05.017 (in press).